

# Revealing the unbinding mechanics of hyaluronan-receptor interactions on live cells

Itzel Garcia-Monge<sup>1,2</sup>  | Ashleigh Goodenough<sup>1,2</sup>  | Cihan Civan Civaş<sup>1</sup>  |  
 Jessica C. F. Kwok<sup>1,3</sup>  | Ralf P. Richter<sup>1,2</sup> 

<sup>1</sup>School of Biomedical Sciences, Faculty of Biological Sciences, University of Leeds, Leeds, UK

<sup>2</sup>School of Physics and Astronomy, Faculty of Engineering and Physical Sciences, Astbury Centre for Structural Molecular Biology, and Bragg Centre for Materials Research, University of Leeds, Leeds, UK

<sup>3</sup>Institute of Experimental Medicine, Czech Academy of Science, Prague, Czechia

## Correspondence

Ralf P. Richter, School of Biomedical Sciences, Faculty of Biological Sciences, University of Leeds, Leeds LS2 9JT, UK.  
 Email: [r.richter@leeds.ac.uk](mailto:r.richter@leeds.ac.uk)

## Funding information

BBSRC, UK, Grant/Award Numbers: BB/X007278/1, BB/R000174/1, BB/R000351/1; CONAHcyT; University of Leeds; Wellcome Trust, Grant/Award Number: WT104918MA

## Abstract

The extracellular matrix polysaccharide hyaluronan (HA) and its receptors are important mediators of cell adhesion and migration, and tissue mechanics. While mechanical forces are clearly important in these processes, there is a lack of methods to study the effect of mechanical forces on individual bonds of HA with its receptors directly on the surface of cells. Here, we present an assay based on atomic force microscopy to probe the frequency of bond formation (along with the receptor surface density) and the mechanical resistance of HA-receptor bonds to a force ramp on live cells. We demonstrate the method using a lymphoma cell line with stably transfected CD44 and one-end anchored HA chains. We validate that HA-CD44 unbinding forces on cells are high compared to their relatively low binding affinity, and that bond rupture is dominated by a single energy barrier. The new live cell single HA chain force spectroscopy assay can be used to reveal the interaction mechanics with CD44 or other receptors in distinct interaction geometries, and adapted for other glycosaminoglycans and their receptors.

## KEYWORDS

CD44, force spectroscopy, hyaluronan, live cell

## INTRODUCTION

Dynamic force spectroscopy can reveal the response of individual molecules, molecular bonds, and multivalent supramolecular interactions to a tensile force.<sup>1–3</sup> It provides information about bond lifetime as a function of an applied constant force (force clamp), or about the magnitude of the force that a bond can withstand when pulled apart at a certain force loading rate (force ramp). From such

analyses, insights into the path of the unbinding process in the energy potential landscape specific to the bond, and into the molecular nature of the bond mechanics,<sup>4</sup> can be obtained. Such information is particularly pertinent for molecular interactions that are subject to mechanical forces in their natural environment, where equilibrium biochemical characteristics such as affinity and (zero-force) association/dissociation rates are not the only determinants of molecular interaction. A case in point is interactions between adhesion

**Abbreviations:** AFM, atomic force microscopy;  $A_{\text{HA}}$ , cell surface area covered by the HA chain; b, biotin; BSA, bovine serum albumin; DAPI, 4',6-diamidino-2-phenylindole; DMEM, Dulbecco's modified Eagle's medium; DPBS, Dulbecco's phosphate-buffered saline;  $d_{\text{rms}}$ , root mean square (rms) distance; FBS, fetal bovine serum; HA, hyaluronan;  $K_d$ , equilibrium dissociation constant;  $k_{\text{eff}}$ , effective spring constant;  $L_c$ , contour length;  $L_p$ , persistence length;  $N_{\text{bonds/curve}}$ , number of bonds per force curve; OEG, oligo(ethylene glycol); QCM-D, quartz crystal microbalance with dissipation monitoring;  $r$ , loading rate;  $R_g$ , radius of gyration; SAM, self-assembled monolayer; SAV, streptavidin;  $v$ , velocity; WLC, worm-like chain; WT, wild type;  $x_b$ , effective width of the energy barrier;  $\tau_{\text{contact}}$ , effective contact time;  $\tau_{\text{dwell}}$ , dwell time at maximal load;  $\tau_0$ , enhanced bond lifetime.

This is an open access article under the terms of the [Creative Commons Attribution](https://creativecommons.org/licenses/by/4.0/) License, which permits use, distribution and reproduction in any medium, provided the original work is properly cited.

© 2024 The Author(s). *Proteoglycan Research* published by Wiley Periodicals LLC.

receptors on the cell surface and their ligands in the surrounding extracellular matrix or on adjacent cells, as these experience and transmit tensile forces when tissues or cells deform.<sup>5</sup>

Hyaluronan (HA) and its cell surface receptors are known to play important roles in cell adhesion and migration.<sup>6,7</sup> HA is a ubiquitous, negatively charged polysaccharide component of extracellular matrix. Individual HA chains are made of a linear sequence of repeating disaccharides of D-glucuronic acid and N-acetyl-D-glucosamine linked by alternating  $\beta$ -1,3 and  $\beta$ -1,4 glycosidic bonds [- $\beta$ (1,4)-GlcA- $\beta$ (1,3)-GlcNAc-]<sub>n</sub>. HA chains are typically large ( $n \gtrsim 10^3$ ), with molecular masses in the MDa range and contour lengths in the  $\mu$ m range. Owing to its large size, a single HA chain can simultaneously engage with many copies of its cell surface receptors or other extracellular HA-binding proteins. CD44, the best-studied cell surface receptor for HA, has been implicated in the adhesion and migration of immune<sup>6-9</sup> and cancer<sup>10-12</sup> cells. Other transmembrane receptors for HA with established or suggested functions in cell adhesion are the lymphatic vessel endothelial receptor 1 (LYVE-1)<sup>6,13</sup> and layilin.<sup>14,15</sup>

Dynamic force spectroscopy was originally established for the analysis of interactions between purified molecules. In this realization, one interaction partner is anchored to a solid support, and the other to a force transducer. Purified molecules and their controlled anchorage to supports or force transducers with defined mechanical properties have the benefit of tight control over the interaction geometry and force balance, thus facilitating the interpretation of the generated data in the context of quantitative theoretical models of bond mechanics.<sup>16</sup> For HA and other members of the family of glycosaminoglycan polysaccharides, such analyses have revealed the unusual mechanics of enzyme/glycosaminoglycan interactions,<sup>17</sup> the mechanisms underpinning mechanical tension in HA-aggregran complexes,<sup>18</sup> and the mechanical strength of bonds between HA and its binding proteins,<sup>19,20</sup> for example.

A persistent question though is if the phenomena observed with isolated molecules are representative of the behavior of these same molecules in their native environment,<sup>21</sup> where receptor density and organization, co-factors and distinct interaction geometries may affect the interaction mechanics. Dynamic force spectroscopy directly on cells overcomes this limitation. Ligand-functionalized nanoscale probes as force transducers have provided detailed insight into the mechanics of molecular interactions at the cell surface, such as the binding of viruses or ligands to cell surface glycans and receptors, and also enabled the mapping of receptor localizations across the cell surface.<sup>21-23</sup> In these studies, ligands are typically attached to the force transducer via a rather short polymer linker with a typical contour length in the range of tens of nanometres to constrain the ligand in a small space.

In previous work, we deployed atomic force microscopy (AFM)-based DFS to probe monovalent and multivalent bonds between hyaluronan and CD44 under force.<sup>19</sup> Using purified CD44 ectodomains anchored to a planar support, and HA polymers anchored with one end to an AFM tip, we showed (i) that individual bonds between HA and CD44 are remarkably resistant to rupture under force (in comparison to their low binding affinity,  $K_d \approx 50 \mu\text{M}$ ), (ii) that the unbinding response in the studied interaction geometry and force

range is governed by a single activation barrier (i.e., well described by the simple interaction model originally developed by Bell and Evans), and (iii) that multiple bonds along a single HA chain rupture sequentially and independently under load. It remained unclear, however, if the findings in this model interaction scenario faithfully mirror the behavior of CD44 on live cells.

Here, we present an assay to analyze the unbinding mechanics of a single HA chain from its receptors on a live cell. The assay deliberately uses long HA chains to probe monovalent and multivalent interactions, distinct from previous force spectroscopy methods on cells with other ligands. We demonstrate the method on AKR1 cells (a lymphoma cell line) with stably transfected CD44. We validate that the HA-CD44 unbinding under force on live cells is qualitatively in line with previous findings for purified receptors.<sup>12</sup> We report reduced bond rupture forces on live cells compared to purified receptors, however, which we propose is due to differences in receptor source and/or glycosylation, highlighting the importance of studying HA-receptor interactions on the corresponding cell surface.

## MATERIALS AND METHODS

### Materials

HEPES buffered-saline (HBS) solution was made of 10 mM HEPES (pH 7.4) and 150 mM NaCl (both Sigma-Aldrich) in ultrapure water.

Streptavidin (SAV; Sigma-Aldrich #S4762) was dissolved in ultrapure water at 1 mg/mL stock concentration. Hyaluronan polymer with a biotin tag at its reducing end (HA-b) and well-defined molecular weight ( $840 \pm 60$  kDa; Select HA-1000; Hyalose) was dissolved in ultrapure water at 1 mg/mL stock concentration without stirring or vortexing. Bovine serum albumin (BSA; Sigma-Aldrich, #A9647) was dissolved in HBS at 1 mg/mL stock concentration. Anti-CD44 antibody IM7 labeled with Alexa Fluor 488 (IM7-AF488; Fisher Scientific, #58-0441-82) was stored at 0.5 mg/mL.

Two di-end functional oligo(ethylene glycol) (OEG) reagents (Polypure) were used for the formation of mixed biotin-presenting self-assembled monolayers (b-SAMs), one made of two EG<sub>7</sub> strands with hydroxyl groups on one end and connected by a disulfide on the other (OEG-disulfide), and the other made of EG<sub>10</sub> with biotin on one end and a thiol on the other (b-OEG-thiol).

### Cell culture

AKR1, a CD44 negative T-cell lymphoma cell line, was stably transfected with either murine wild type CD44 (AKR1 CD44<sup>+</sup> WT) or the R41A mutant of CD44 (AKR1 CD44<sup>+</sup> R41A), and kindly provided by Dr. Robert Hyman (The Salk Institute for Biological Studies).<sup>24-26</sup>

The cells were cultured in suspension in Dulbecco's modified Eagle's medium (DMEM; Gibco, #11584486), supplemented with 10% (v/v) heat-inactivated fetal bovine serum (FBS; Gibco, #11550356), and 1% (v/v) of a mixture of penicillin (10,000 U/mL),

streptomycin (10,000 mg/ml), and Gibco Amphotericin B (25 µg/mL) (PSF; Gibco, #11570486) at 37°C, 5% CO<sub>2</sub> in T25 flasks (Thermo Fisher #156367). The cells were passaged twice a week.

## Cell adhesion for live cell AFM analysis and optical imaging

Sterile glass-bottomed Petri dishes (Fluorodish; World Precision Instruments, #fd35-100) were filled with 3 mL of DMEM and incubated at 37°C for 20 min. Approximately 35,000 AKR1 CD44<sup>+</sup> cells were added per dish and allowed to adhere at 37°C and 5% CO<sub>2</sub> for 20 min. DMEM with unattached floating cells was then aspirated and replaced with fresh DMEM before further analysis of the adhered cells.

## Immunocytochemistry

Cells were plated on clean and sterile glass coverslips (SLS Select Coverslips #1.5, 13 mm diameter, #MIC3336) placed in 24-well plates (Sarstedt) at a density of approximately 20,000 cells per coverslip, following the above-described procedure. Cells were gently rinsed with Dulbecco's phosphate-buffered saline (DPBS; Sigma-Aldrich), fixed with 4% (w/v) paraformaldehyde (PFA; VWR International) for 15 min at room temperature while on a shaker, and rinsed with DPBS before staining. Cells were incubated with IM7-AF488 (1:5000 dilution) and 4',6-diamidino-2-phenylindole (DAPI; Boster Biological Technology; 1:3000 dilution) in DPBS with 1% (v/v) FBS at 4°C overnight in the dark and rinsed with 1× Trizma base (TNS; Sigma-Aldrich) three times every 10 min at room temperature on a shaker. Coverslips were mounted on a clean glass slide with FluorSave (Sigma-Aldrich) and left to dry overnight at room temperature in the dark before imaging.

## Optical microscopy

The morphology of adhered live cells was assessed by phase contrast microscopy using an Axio Observer 7 inverted microscope (Zeiss) with environmental enclosure (37°C), an EC Plan-Neofluar 40×/0.75 Ph2 objective (ZEISS), and a scientific CMOS camera (Orca Fusion, Hamamatsu) at 0.102 µm pixel resolution. Twenty images were taken at different areas of the coverslip surface at desired time points.

Stained and fixed cells were imaged using an LSM880 inverted laser scanning microscope (Zeiss), a Plan-Apochromat 40×/1.4 Oil DIC objective, excitation wavelengths of 488 and 405 nm, and pinhole sizes of 0.79 Airy units (AU) and 0.93 AU, respectively, for IM7-AF488 and DAPI. All images were analyzed and processed using Fiji software.<sup>27</sup>

## Flow cytometry

Flow cytometry was performed with a Cytoflex S (Beckman Coulter) using 488 nm excitation and a 525/40 bandpass filter and CytExpert

software (Life Sciences). 10,000 events were acquired per cell preparation (see Supporting Information S1: Figure S2 for details).

## Single HA chain force spectroscopy

Force spectroscopy was performed on a NanoWizard IV (Bruker) AFM combined with an inverted IX73 optical microscope (Olympus).

Gold-coated AFM probes (NPG-10; Bruker) with a nominal spring constant of 0.06 N/m were used; the real spring constant was validated by the thermal noise method.<sup>28</sup> The probe surface was first functionalized with a b-SAM. To this end, probes were treated with UV/ozone (UVO Cleaner, Jelight Company) for 30 min, immersed in an ethanol solution of 0.98 mM OEG-disulfide and 0.02 mM b-OEG-thiol overnight at 4°C, rinsed with ethanol, and blow-dried with N<sub>2</sub> gas. b-SAM coated probes were sequentially incubated in 20 µg/mL SA<sub>v</sub> (20 min) and 2 µg/mL HA-b (840 kDa; 6 min) in HBS, with intermittent rinses in HBS and avoiding drying. This procedure leads to sparse coverage of the probe with one-end anchored HA chains, enabling only one or at most very few HA molecules to contact the cell surface.<sup>19</sup>

Cells adhered to glass-bottomed Petri dishes and maintained in DMEM were exposed to ambient air at 37°C (with a JPK Petri-DishHeater; Bruker) during analysis. The functionalized AFM probe was positioned near a cell of interest, without touching the cell or the glass surface. Atomic force and optical micrographs were aligned using the DirectOverlay function in the JPK Nanowizard Control software. Viable and well-isolated cells were selected for analysis. Around six different cells were analyzed per velocity, acquiring several 100 force versus displacement curves on two distinct positions (separated by 4 µm) near the center of each cell.

Force versus displacement curves were acquired at selected approach and retract velocities ( $v = 1\text{--}10\ \mu\text{m/s}$ ) with a sampling rate of 5 kHz resulting in a noise in the force of approximately 13 pN (standard deviation). The maximal applied load was 300 pN, and the dwell time on the cell surface was kept minimal, except at  $v = 10\ \mu\text{m/s}$  where it was set to 50 ms. Force versus displacement curves were converted to force versus distance curves, and further analyzed, with JPK Data Processing software (Bruker). Where appropriate, force versus distance retract data were fitted using the worm-like chain (WLC) model<sup>29</sup> to extract the apparent contour length ( $L_{c,app}$ ) and persistence length ( $L_{p,app}$ ) of the stretched chain and the bond rupture force  $F$ . The effective spring constant  $k_{eff}$  was calculated as the slope of the force versus distance relationship ( $k_{eff} = \frac{dF}{dx}$ , determined through the WLC model fit) at the point of bond rupture, and the instantaneous loading rate was taken as  $r = k_{eff}v$ .

## RESULTS

The experimental approach combines an AFM probe functionalized with hyaluronan and live cells adhered to a glass coverslip, as schematically shown in Figure 1.

We first validated the functionalization of the AFM probe (Supporting Information S1: Figure S1) as had been previously established<sup>19,20</sup> (Figure 1A): HA was anchored by a biotin moiety at its reducing end to streptavidin, which was itself bound by at least two of its four biotin-binding sites<sup>30</sup> to a biotin-presenting self-assembled monolayer (b-SAM) of oligo(ethylene glycol) molecules, which in turn were covalently bonded by their terminal thiol moieties to the gold-coated AFM tip. This mode of HA attachment provides tensile forces on HA-receptor interactions in a well-defined direction (i.e., pulling from the reducing end), and can probe the unbinding mechanics of HA-CD44 interactions with minimal risk for breakage of the anchorage itself.<sup>19</sup> The flexible HA chains had a defined contour length of  $L_c = 2.1 \pm 0.2 \mu\text{m}$  and were sparsely anchored to the AFM

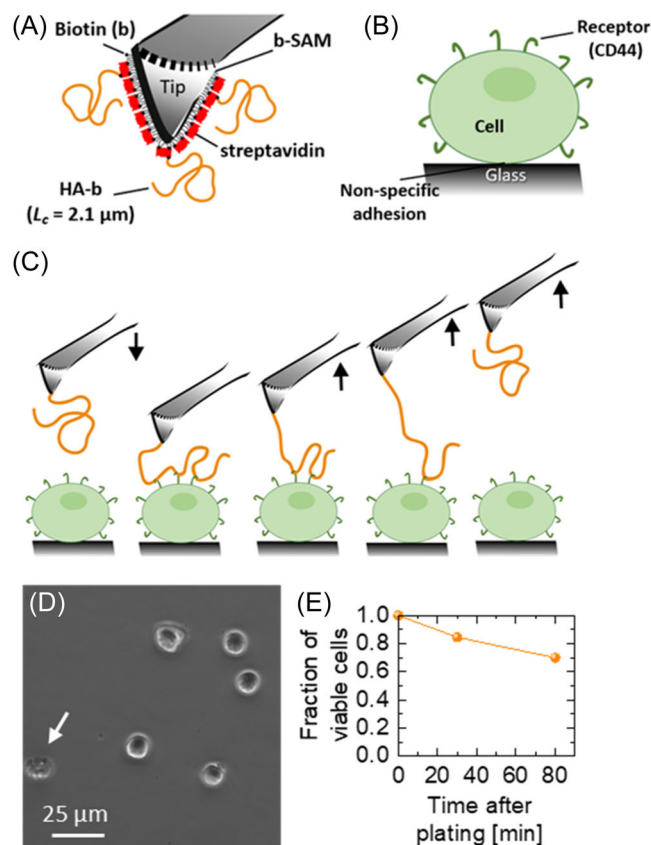


**FIGURE 1** Schematic representations (not to scale) of single HA chain force spectroscopy on cells. (A) AFM probe presenting HA chains (here 840 kDa, corresponding to contour length  $L_c = 2.1 \mu\text{m}$ ) anchored by their reducing end. (B) Live cells (here AKR1 CD44<sup>+</sup>) attached to a glass surface through nonspecific adhesion. (C) Expected binding and unbinding processes. The AFM tip is lowered to the cell, enabling the formation of one or more HA-receptor bonds, and when the tip retracts, unbinding forces are measured. (D) Representative phase contrast image of AKR1 CD44<sup>+</sup> WT cells adhered on a plain glass surface (80 min after plating). Viable cells present a clear round shape; a few cells (white arrow) exhibited a more complex shape and less contrast, and are likely dying or dead. (E) Fraction of viable cells as a function of time (averaged across an area of  $0.6 \text{ mm}^2$ ). AFM, atomic force microscopy; HA, hyaluronan; WT, wild type.

probe, thus forming random coils with a radius of gyration  $R_g = 75 \text{ nm}$ , that is, sufficiently large for an individual HA chain to sample an area on the cell surface on the order of  $10^4 \text{ nm}^2$ .<sup>19</sup> In addition, the streptavidin-on-b-SAM coating minimized nonspecific binding.

We used AKR1 cells, a CD44-negative T-cell lymphoma cell line, as a cell model. AKR1 cells were stably transfected with wild-type CD44 (AKR1 CD44<sup>+</sup> WT) or with the R41A mutant of CD44 (AKR1 CD44<sup>+</sup> R41A) with a much reduced HA binding capacity<sup>31</sup> as a control. CD44-transfected AKR1 cells have previously been established as a good model for the mechanistic analysis of HA/CD44 interactions in a cellular context.<sup>24–26</sup>

## Establishing force spectroscopy on live cells

We serendipitously observed that AKR1 cells (which are naturally cultured in suspension) adhere spontaneously to plain glass surfaces. The majority of adhered cells remained viable and minimally perturbed in their round morphology 80 min after plating (Figure 1D,E), thus providing a robust source of cells during the AFM analysis time of typically a few hours. Flow cytometry confirmed that cells transfected with WT and R41A CD44, respectively, were each a single population of CD44 presenting cells (Supporting Information S1: Figures S2 and S3). Immunocytochemistry showed that CD44 is quite evenly distributed across the cell surface (Supporting Information S1: Figure S4).

## Curation of force versus distance curves (I)—Qualitative inspection

We thus proceeded to force spectroscopy analysis by AFM. A coupled optical microscope aided the positioning of the AFM probe (Figure 2A, inset) approximately centrally above a cell. The tip was then approached to the cell until a set compression force of 300 pN was reached. Representative force versus distance curves, captured on subsequent retraction of the tip from the cell, are shown in Figure 2B,C.

Force curves exhibited a variety of shapes. A good proportion exhibited one or few characteristic adhesion peaks of typically a few 10 pN in magnitude composed of a gradual increase in force with distance followed by an abrupt decrease (Figure 2B). We attribute these responses to the stretching of an HA chain followed by the rupture of a bond between HA and the cell surface. These responses are the most relevant and were analyzed in detail (vide infra). A large fraction (>70%) of the force curves exhibited no notable features at all (Figure 2C, bottom), demonstrating that the likelihood of HA-receptor interaction upon the brief encounter of HA on the AFM tip with the cell is relatively low. Reassuringly, they also demonstrated a low level of undesired nonspecific interactions.

Some force curves, however, revealed that other interactions are occasionally occurring between the AFM tip and the cell. In particular, some force curves evidenced a constant pulling force of typically

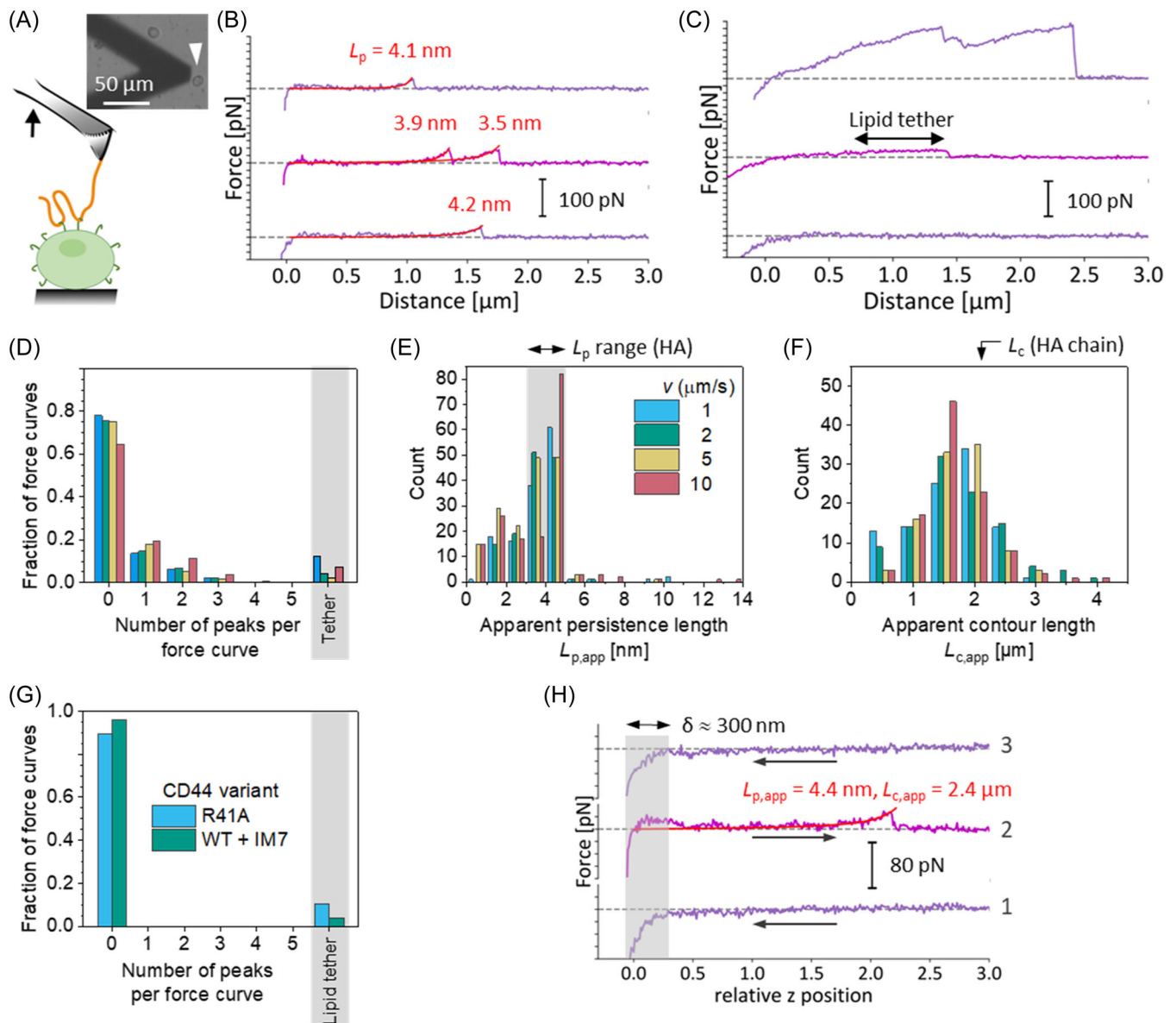


**FIGURE 2** Identifying force curves that represent CD44 unbinding from a single HA chain. (A) Schematic representation of the assay; inset shows AFM cantilever (dark > shape) on a surface with adhered cells (white arrowhead points to an example). (B and C) Representative force curves obtained with HA-functionalized AFM tips on AKR1 CD44<sup>+</sup> WT cells: (B) Three force versus distance curves (retract parts only; velocity  $v = 5 \mu\text{m/s}$ ; thin magenta lines) showing one (top and bottom) or two (middle) HA chain stretching and unbinding responses (WLC model fits and resulting apparent persistence lengths  $L_{p,app}$  in red). (C) Three additional force versus distance curves (retract parts only;  $v = 5 \mu\text{m/s}$ ) that do not represent specific interactions of the HA chain with the cell: (bottom) no appreciable adhesive interactions evidence lack of receptor binding; (middle) extended regime of a constant adhesive force (black double arrow), followed by sharp unbinding are likely due to plasma membrane tether formation and rupture; (top) extensive adhesive interactions, up to several 100 pN, indicate nonspecific interactions of the AFM tip with the cell. (D–F) Detailed analysis of force curves representing unbinding of HA chains from AKR1 CD44<sup>+</sup> WT cells for the four velocities tested (as indicated in (E)): (D) Histogram of the number of valid rupture events per force curve; force curves with tethers were included as a separate class in this analysis (highlighted in gray). Histograms of the apparent persistence lengths  $L_{p,app}$  (E), and contour lengths  $L_{c,app}$  (F), as obtained from WLC fits to valid rupture events. The  $L_p$  range considered to represent single HA chain stretching is highlighted in gray (in (E)), and the contour length of the HA chains with an arrow (in (F)). (G) Histograms (from  $n = 150$  force curves per condition) of the number of rupture events per force curve for an HA-presenting AFM tip on (i) AKR1 CD44<sup>+</sup> WT cells in the presence of the anti-CD44 antibody IM7 (10  $\mu\text{g/mL}$ ; green), and (ii) AKR1 CD44<sup>+</sup> R41A cells (blue). (H) Three consecutive force traces (from bottom to top; approach—purple, retract—magenta;  $v = 5 \mu\text{m/s}$ ) acquired on the same spot illustrate the level of cell indentation  $\delta$  (highlighted in gray) and that the cell surface recovers its position rapidly after pulling on CD44 with HA (as evidenced by a rupture event in the retract curve, with WLC fit and results indicated in red). For enhanced clarity, force versus distance data were downsampled to a rate of 500 Hz (resulting in noise in force of approximately 4 pN standard deviation) for their display in panels (B, C, and H). AFM, atomic force microscopy; HA, hyaluronan; WLC, worm-like chain; WT, wild type.

a few 10 pN over distances of hundreds of nanometres (Figure 2C, middle). A likely explanation is the formation of lipid membrane tethers. Indeed, such responses arise upon pulling lipid membrane tubes (or rod-like micelles) using the cell's membrane reservoir as a lipid supply.<sup>32–34</sup> We sometimes also found much stronger adhesive interactions, reaching >100 pN in force and extending over hundreds of nanometres (Figure 2C, top). These responses were not usually observed with a freshly prepared probe but became prominent after hundreds of force curves had been acquired across several cell locations, indicating that they represent the result of tip contamination. Consequently, these force curves were discarded from further analysis.

Figure 2D provides a statistical analysis of the types of force curves obtained across the range of tip approach and retract velocities investigated. While between 60% and 80% of all valid force curves showed zero rupture events, productive interactions via HA typically led to force curves with one or two, rarely three or four, and never more than four rupture events. These findings are consistent with a stochastic engagement of CD44 cell surface receptors with HA, with no, one, or several bonds being formed with distinct probabilities. A Poisson distribution reproduced the incidence of rupture events rather well, though a somewhat larger than predicted incidence of two or more bonds suggested that the likelihood for a second bond (and further bonds) is enhanced after the first bond has formed (Supporting Information S1: Figure S5).

A couple of controls confirmed that the productive interaction of CD44 and HA is strictly required for the force responses shown in Figure 2B: replacing wild-type CD44 with the R41A mutant in the AKR1 cell context (Figure 2G) virtually eliminated this type of force responses. Interestingly, IM7 had the same effect on AKR1 CD44<sup>+</sup> WT cells (Figure 2G), even though this antibody has been reported for a rather moderate HA-blocking activity.<sup>35</sup> Some instances of lipid tether formation were though observed in both these control interaction scenarios (Figure 2G), at frequencies broadly comparable to the original assay (Figure 2D). This suggests that the lipid tether formation is unrelated to HA-CD44 bond formation, and instead arises from spurious nonspecific interactions of the AFM probe with the cell surface. Force curves with lipid tethers were therefore also discarded from further analysis.

## Curation of force versus distance curves (II)— Quantitative analysis of HA chain stretching

To gain further insight into the nature of the productive interactions with HA, all valid force peaks were analyzed using the WLC model. The WLC model describes the resistance of a flexible chain to stretching, which depends on thermal energy  $k_B T$  (reflecting the entropic nature of the resistance to stretching), the persistence length  $L_p$  (a measure of chain stiffness), and the contour length  $L_c$  of the chain segment being stretched:

$$F = -\frac{k_B T}{L_{p,app}} \left[ \frac{1}{4} \left( 1 - \frac{x}{L_{c,app}} \right)^{-2} + \frac{x}{L_{c,app}} - \frac{1}{4} \right], \quad (1)$$

where  $F$  is the tensile force and  $x$  the distance. The WLC model reproduced most of the force peaks well (Figure 2B, red lines).  $L_{p,app}$  and  $L_{c,app}$  were the sole adjustable parameters, where the subscript “app” denotes that some values may be apparent rather than real (vide infra). Histograms of the results are shown in Figure 2E,F.

The apparent persistence lengths showed a clear maximum of around 4 nm for all approach/retract velocities tested (Figure 2E and Supporting Information S1: Figure S6). This value agrees very well with the persistence length of  $L_p = 4.1$  nm previously established for HA polymers through force spectroscopy.<sup>19</sup> Moreover, the standard deviations in the persistence length (ranging from 0.3 to 1.5 nm depending on velocity; Supporting Information S1: Figure S6) were broadly comparable with the previous work.<sup>19</sup> Thus, individual HA chains were stretched, as indeed desired, in the vast majority of force peaks.

Figure 2E though also reveals a sub-population of force peaks with an apparent persistence length substantially smaller than 4 nm. Quite possibly, these events are due to more than one HA chain being pulled simultaneously; for example, two HA chain segments of equal length stretched in parallel would double the force for any given distance, thus giving rise to an apparent persistence length of  $L_{p,app} = L_p/2 = 2$  nm. Similarly, two HA chain segments of unequal length or attached at different locations on the AFM tip when pulled together would lead to a reduced apparent persistence length. Very rarely, we also observed apparent persistence lengths that were much larger than 4 nm, suggesting occasional more complex interactions.

We note that the spread of persistence lengths remained broadly consistent while probing a given cell with a given AFM tip (Supporting Information S1: Figure S7), that is, no appreciable changes were observed leading up to the time when the stronger adhesive interactions became apparent that indicated tip contamination (Figure 2C, top curve). This control illustrates that the probing of HA/receptor interactions is not affected by any potential modification of the tip before the onset of detectable contamination in the force curves.

Going forward, we used the apparent persistence length as a quality control criterion: rupture events associated with apparent persistence lengths below 3 nm and above 5 nm were discarded as these may not represent individual HA-CD44 bonds, while events with  $L_{p,app} = 4 \pm 1$  nm were retained recognizing the noise in the fitting. Indeed, neither the rupture force nor the apparent contour length nor the loading rate showed a clear correlation with  $L_p$  within the  $4 \pm 1$  nm range (Supporting Information S1: Figure S7), providing confidence in the robustness of the data.

The apparent contour lengths were rather broadly distributed (Figure 2F), indicating that cell-surface CD44 can bind anywhere along the HA chain contour. Most of the data were within the total contour length of the HA chains ( $L_p = 2.1 \pm 0.2 \mu\text{m}$ ), as expected. Intriguingly, the apparent contour lengths occasionally exceeded the expected range, reaching values as large as  $4 \mu\text{m}$ . This unexpected

observation hinted at an added element of complexity when pulling with HA on receptors on the surface of a live cell.

### The cell surface deforms upon HA pulling on single CD44 receptors

We hypothesized that the excessive apparent contour length might arise from the cell surface with its receptors moving out of the plane while the HA chain is being pulled. To test this hypothesis, we inspected the approach and retracted parts of force curves obtained consecutively on the same (lateral) position on a cell before, during, and after a rupture event (Figure 2H). Focusing on the approach parts, it can be seen that compressive forces of a few 10 pN after contact formation are sufficient to indent the cell by a few 100 nm. Further, a comparison of the approach and retract parts of a force curve (compare traces 1 and 2 in Figure 2H) revealed hysteresis, indicating that the cell surface relaxes upon release of the compressive force albeit not quite at the rate of the retracting AFM tip. This implies that the cell surface is not stationary but continues to move outward when the AFM tip starts to pull on an engaged HA chain. Moreover, it also provides indirect evidence that an HA chain would be capable of actively displacing the cell membrane substantially (i.e., by hundreds of nanometres) while pulling on a CD44 receptor, as the pulling forces exerted via the HA-CD44 bond are of a similar order of magnitude as the compressive forces upon approach (albeit in opposite direction). Lastly, a comparison of the approach parts of two consecutive force curves (compare traces 1 and 3 in Figure 2H) with an intermittent rupture event (trace 2) reveals comparable contact point positions, indicating that the cell membrane relaxes fully to its original position within the time required for the AFM tip to approach the cell again.

While this analysis revealed the soft and viscoelastic nature of the cell surface, the movement of the cell membrane during the pulling process will also impact the exact shape of the force peaks. Although such an effect is not considered in the WLC model and thus could be problematic, it does in practice not appear to have an excessive impact on the apparent persistence length (Supporting Information S1: Figure S8). As such, it also does not impact the quantification of the rupture forces and the instantaneous loading rates. These two parameters were considered next to gain insight into the mechanics of HA-CD44 bonds on cells.

### Single HA-CD44 bond rupture forces and kinetic parameters on cells

Histograms of all rupture forces obtained following the curation of force curves evidence relatively broad yet unimodal distributions for all retract velocities (Figure 3A). Gaussian fits were used as a simple approach to quantify the mean and width of the distributions. Similarly, loading rates  $r = k_{\text{eff}}v$  were extracted from the effective spring constants  $k_{\text{eff}}$  (corresponding to the slope of the WLC fits at the point

of bond rupture) and the retract velocities  $v$  and Gaussian fits were used to quantify the mean and width of the loading rates for each velocity (Supporting Information S1: Figure S9). It can be seen that HA-CD44 bonds are quite resistant to force, with tens of pN required for bond rupture for the range of loading rates investigated.

Figure 3B (black symbols) shows the rupture force as a function of the logarithm of the loading rate and represents the main results of our analysis. A clear linear trend is observed in this semi-logarithmic plot. Such a dependence matches expectations of the Bell-Evans model, indicating that the unbinding process of HA from CD44 is

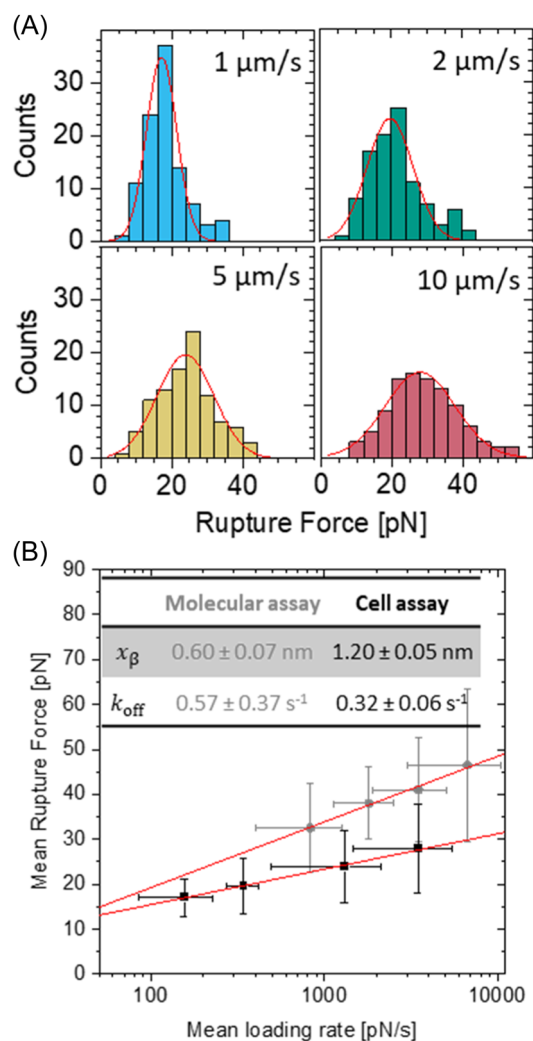


**FIGURE 3** Rupture force distributions demonstrate HA-CD44 bond rupture on cells is well-described by the Bell-Evans model. (A) Histogram of rupture forces as a function of the retract velocity (as indicated) with Gaussian fits (red curves). (B) Mean rupture forces ( $\pm$ standard deviations obtained from the Gaussian fits in (A)) as a function of the mean loading rates ( $\pm$ standard deviations; see Supporting Information S1: Figure S9) obtained on AKR1 CD44<sup>+</sup> WT cells (black squares). Previously reported results<sup>19</sup> for purified receptors anchored to an artificial support (gray circles) are shown for comparison. The straight lines (red) represent the best fits with the Bell-Evans model, with the resulting kinetic parameters shown in the table (inset). HA, hyaluronan; WT, wild type.

dominated by a single energy barrier. A fit with the Bell–Evans model<sup>3,36,37</sup>:

$$F = \frac{k_B T}{x_\beta} \ln \left[ \frac{r x_\beta}{k_{\text{off}} k_B T} \right], \quad (2)$$

revealed  $x_\beta = 1.20 \pm 0.05$  nm as the width of the energy barrier, and  $k_{\text{off}} = 0.32 \pm 0.06$  s<sup>-1</sup> as the dissociation rate constant in the limit of zero force (Figure 3B), thus providing a quantitative definition of the energy barrier for an HA-CD44 bond when exposed to tensile stress from the HA chain's reducing end.

### Estimating CD44 cell surface density by force spectroscopy

Owing to the large number of binding sites on a single HA chain, the frequency of bond formation in force spectroscopy can also provide some insight into the CD44 density on the cell surface, as follows. From a zero-force unbinding rate constant  $k_{\text{off}} = 0.32$  s<sup>-1</sup> (Figure 3B) and an affinity  $K_d \approx 50$  μM,<sup>38</sup> we estimate a binding rate constant  $k_{\text{on}} = k_{\text{off}}/K_d \approx 6.4 \times 10^3$  M<sup>-1</sup> s<sup>-1</sup>. From the radius of gyration ( $R_g \approx 75$  nm) and contour length ( $L_{c,\text{HA}} = 2.1$  μm) of the HA chain and considering that the CD44 binding site on HA is 4 disaccharides long<sup>39</sup> ( $L_{c,\text{bs}} = 4$  nm), we estimate the concentration of CD44 binding sites in the HA coil as  $c_{\text{bs}} \approx L_{c,\text{HA}}/L_{c,\text{bs}} R_g^{-3} N_A^{-1} \approx 2.2$  mM. From the approach and retract velocity ( $v = 1$ – $10$  μm/s), the dwell time at maximal load ( $\tau_{\text{dwell}} = 0$  s for  $v = 1$ – $5$  μm/s, and  $0.05$  s for  $v = 10$  μm/s), and an interaction distance  $R_g$ , we estimate an effective contact time of the HA chain with the cell surface on the order of  $\tau_{\text{contact}} \approx R_g/v + \tau_{\text{dwell}}$ . Ultimately, from the frequency of bonds per force curve ( $N_{\text{bonds/curve}}$ ; Figure 2D), the cell surface area covered by the HA chain ( $A_{\text{HA}} \approx R_g^2$ ) and the above parameters, we estimate the root mean square (rms) distance between CD44 receptors as  $d_{\text{rms,CD44}} \approx \sqrt{R_g^2 k_{\text{on}} c_{\text{bs}} \tau_{\text{contact}} / N_{\text{bonds/curve}}}$ . With this approach,  $d_{\text{rms,CD44}}$  estimates in the range of 47 to 135 nm were obtained depending on the retract velocities. These values are broadly consistent with levels of native CD44 expression in cells.<sup>40,41</sup>

## DISCUSSION

We have successfully established an assay to probe, with high specificity, the interaction mechanics between hyaluronan and its protein receptors on live cells. Force spectroscopy quantified the tensile strength of individual HA-CD44 bonds in a cellular context and also estimated the CD44 surface density on AKR1 cells.

### Comparing HA-CD44 interaction on live cells versus immobilized receptor ectodomains

The results showed that HA-CD44 interactions can form at any location along the HA polymer chain; when multiple CD44 receptors

engage with the HA chain, these rupture sequentially and independently upon application of a tensile force at the end of the HA chain. Qualitatively, the results presented here for CD44 on live cells were similar to previously reported findings with purified CD44 ectodomains anchored to solid or fluid supports.<sup>19</sup> While the results verified the methods we used for cell analysis, these findings also demonstrate that the unbinding mechanics of CD44 from HA polymers are not fundamentally impacted by the cell surface environment.

A quantitative comparison, however, reveals some notable differences in the unbinding mechanics of individual HA-CD44 bonds. Figure 3B shows previously published data<sup>19</sup> for the interaction of HA with recombinant CD44 ectodomains (made in CHO cells) on a solid support (*gray symbols*) alongside our new data for full-length CD44 on live cells (*black symbols*). While both data sets are well-described by the Bell–Evans model, evidencing that the force response is dominated by a single energy barrier, the mean rupture forces were smaller on cells than on solid supports over the range of loading rates accessed experimentally.

This difference may imply a specific impact of the mechanical environment of the cell on the HA-CD44 binding strength. The flexibility of the lipid membrane or the cell body, for example, might influence force transmission through the HA/CD44 bond, although this effect seems unlikely considering that CD44 anchors to the cell membrane through a single transmembrane helix and that the surface attachment for isolated CD44 ectodomains in our previous work was designed to reproduce the anchorage orientation.

It seems more likely that the quantitative differences in the force response reflect on subtle biochemical variations in CD44. The binding strength is known to be affected by the glycosylation of CD44,<sup>24,38,40,42</sup> and it is quite possible that CD44 expressed by AKR1 versus CHO cells have distinct glycosylation influencing their binding to HA. Indeed, the twofold variations in  $k_{\text{off}}$  observed in our experiments (Figure 3B, *inset*) are relatively modest compared to the variations in  $K_d$  by up to sevenfold that have previously been reported for various CD44 constructs with distinct glycosylation levels<sup>24</sup>; see fig. 5 in Reference 42 for details. Moreover, AKR1 cells expressed murine CD44, whereas ectodomains of human CD44 were used in the earlier work.<sup>19</sup> Finally, it is in principle also possible that other cell surface components impact the HA binding activity of CD44. These distinctive molecular features may well explain the observed differences, and highlight the importance of testing interactions on the cells of interest to assess or confirm specific functions.

### Mechanical responses may be sensitive to the CD44 variant and HA-CD44 interaction geometry probed

Most prominently, a twofold reduced slope in the dependence of the mean rupture force on the loading rate for murine CD44 on AKR1 cells translates into a twofold increase in the effective width of the energy barrier  $x_\beta$  compared to human CD44 from CHO cells (Figure 3B, *inset*). In contrast, the zero-force unbinding rate constant  $k_{\text{off}}$  showed a tendency to decrease (Figure 3B, *inset*), implying an

enhanced bond lifetime  $\tau_0 = k_{\text{off}}^{-1}$  in the absence of a force. Together, this means that the applied force dictates which of the two CD44 variants forms more stable bonds: bond lifetimes  $\tau(F) = k_{\text{off}}^{-1} e^{-F x_p / (k_B T)}$  are enhanced for murine CD44 on AKR1 cells at low forces but for human CD44 from CHO cells at high forces. From the data in Figure 3B (inset), one can estimate the transition between these regimes to occur at  $F_{\text{trans}} \approx 4$  pN with a bond lifetime  $\tau(F_{\text{trans}}) \approx 1.0$  s.

This finding raises the intriguing possibility that the mechanical response of HA-CD44 bonds may be differentially regulated (e.g., through glycosylation) depending on the cell type and cell environment. This hypothesis can be tested in further single HA chain force spectroscopy experiments on cells with natively expressed CD44, varying the cell type and/or the CD44 glycosylation.

We note here that the mechanical responses of biomolecular interactions are known to depend quite sensitively on the direction of the applied force.<sup>43,44</sup> We have here only explored the response to pulling the HA chain at the reducing end. Future work should explore if pulling at the nonreducing end, or simultaneously at both chain ends, leads to distinct responses. In this context, it will be particularly interesting to see if evidence for “catch bonds” (i.e., unusual bonds for which the lifetime increases with force over a certain force range) can be obtained. Although catch bonds have been proposed for CD44 and HA based on computer simulations and experimental work with large ensembles of bonds,<sup>10,45</sup> such a behavior remains to be demonstrated at the level of individual HA-CD44 bonds. Instead, our data indicate that conventional ‘slip bonds’ (for which the lifetime decreases with force) are formed on pulling from the reducing end of the HA chain, at least for forces exceeding 10 pN.

### Applications of single glycosaminoglycan chain force spectroscopy on cells

Our work provides a new tool for the direct analysis of individual HA-receptor interactions on the surface of live cells. Future work can explore the interaction mechanics for CD44 (as outlined above) as well as other HA receptors. Of particular interest will be LYVE-1, given its role (along with CD44) as an adhesion receptor essential for the migration of dendritic cells and macrophages from interstitial tissues into the lymphatics (as part of the adaptive immune response).<sup>13,46,47</sup> Further, the interaction mechanics of layilin<sup>14</sup> are currently unknown and worth exploring. Thanks to the high specificity of interactions demonstrated here, the assay may also be used to probe for the presence of other (yet unknown) HA-binding proteins on cell surfaces.

More widely, the assay can also be adapted to probe interaction mechanics of other glycosaminoglycans such as chondroitin sulfate or heparan sulfate with their cell surface receptors (e.g., the chondroitin sulfate proteoglycan receptors PTP $\delta$  or LAR on neurons) or binding partners residing in the cellular glycocalyx. It will here also be interesting to explore the on-cell interaction mechanics of clearance receptors, such as the HA receptor for endocytosis (HARE),<sup>48</sup> for HA<sup>20</sup> and other glycosaminoglycans,<sup>49</sup> as the process of extracellular

matrix polysaccharide clearance is likely to expose the bonds to mechanical stress. Such assays would benefit from further development of designer glycosaminoglycans chains that present chemically defined oligo- or polysaccharides (as interaction partners) linked via a preferably long and inert polymer chain (as a mechanically defined force transducer) to the AFM tip.

## CONCLUSION

In summary, we have presented a new force spectroscopy assay to analyze the unbinding mechanics of individual HA-receptor bonds on live cells. Using CD44 on a stably transfected cell line, we have demonstrated the feasibility of the assay. The results confirm that the HA-CD44 unbinding mechanics are qualitatively similar on cell surfaces and for purified ectodomains anchored to artificial surfaces, with bond unbinding dictated by a single energy barrier, and multiple bonds per HA chain rupturing sequentially and independently under load. This comparison has also highlighted notable differences in the magnitude of the force response depending on the CD44 variant and expression context, which are worthy of further investigation given the diverse implications of CD44 in cell adhesion and migration processes. The method, which also provides an estimate of the receptor surface density, can now also be used to probe the interaction of other receptors with HA and other glycosaminoglycans.

### AUTHOR CONTRIBUTIONS

**Itzel Garcia-Monge:** Methodology; investigation; validation; visualization; formal analysis; writing—original draft; writing—review and editing; funding acquisition. **Ashleigh Goodenough:** Writing—review and editing; methodology. **Cihan Civan Cıvaş:** Methodology; writing—review and editing. **Jessica C. F. Kwok:** Methodology; writing—review and editing; supervision. **Ralf P. Richter:** Conceptualization; methodology; writing—original draft; writing—review and editing; supervision; funding acquisition; validation; formal analysis; visualization.

### ACKNOWLEDGMENTS

The authors thank Dr. Robert Hyman from The Salk Institute for Biological Studies (La Jolla, CA, USA) for kindly providing the AKR1 cells used for this study, and Profs. Caroline Milner and Anthony J. Day (University of Manchester, UK) for support with access to the cells and guidance with cell culture. The authors thank Drs. Sally Boxall and Ruth Hugues from the Bioimaging Facility at the Faculty of Biological Sciences, University of Leeds, for their support and assistance with flow cytometry and confocal microscopy, and Lekshmi Kailas from the AFM Facility at the School of Physics and Astronomy, University of Leeds, for AFM support. This work was supported by a Research Grant (BB/X007278/1) and an Equipment Grant (BB/R000174/1) from the BBSRC, UK (to RPR), a PhD scholarship by CONAHCyT and the University of Leeds (to IGM), and equipment funding by the Wellcome Trust (WT104918MA) and the BBSRC (BB/R000351/1) to the Bioimaging Facility.

## CONFLICT OF INTEREST STATEMENT

The authors declare no conflict of interest.

## DATA AVAILABILITY STATEMENT

The data that supports the findings of this study are available in the Supporting Information of this article.

## ETHICS STATEMENT

The authors have nothing to report.

## ORCID

Itzel Garcia-Monge  <https://orcid.org/0009-0002-6469-5908>

Ashleigh Goodenough  <https://orcid.org/0000-0003-2431-4891>

Cihan Civan Civaş  <https://orcid.org/0000-0002-3771-5814>

Jessica C. F. Kwok  <https://orcid.org/0000-0002-9798-9083>

Ralf P. Richter  <http://orcid.org/0000-0003-3071-2837>

## REFERENCES

- [1] A. Alessandrini, P. Facci, *Meas. Sci. Technol.* **2005**, *16*, R65.
- [2] R. García, *Surf. Sci. Rep.* **2002**, *47*, 197.
- [3] M. L. Hughes, L. Dougan, *Rep. Prog. Phys.* **2016**, *79*, 076601.
- [4] B. Liu, W. Chen, C. Zhu, *Annu. Rev. Phys. Chem.* **2015**, *66*, 427.
- [5] K. Ley, C. Laudanna, M. I. Cybulsky, S. Nourshargh, *Nat. Rev. Immunol.* **2007**, *7*, 678.
- [6] L. A. Johnson, D. G. Jackson, *Cells* **2021**, *10*, 2061.
- [7] B. McDonald, P. Kubes, *Front. Immunol.* **2015**, *6*, 68.
- [8] H. C. DeGrendele, P. Estess, M. H. Siegelman, *Science* **1997**, *278*, 672.
- [9] L. A. Johnson, S. Banerji, B. C. Lagerholm, D. G. Jackson, *Life Sci. Alliance* **2021**, *4*, e202000908.
- [10] C. Christophis, I. Taubert, G. R. Meseck, M. Schubert, M. Grunze, A. D. Ho, A. Rosenhahn, *Biophys. J.* **2011**, *101*, 585.
- [11] U. Richter, D. Wicklein, S. Geleff, U. Schumacher, *Histochem. Cell Biol.* **2012**, *137*, 687.
- [12] L. T. Senbanjo, M. A. Chellaiah, *Front. Cell. Dev. Biol.* **2017**, *5*, 18.
- [13] D. G. Jackson, *Front. Immunol.* **2019**, *10*, 471.
- [14] P. Bono, K. Rubin, J. M. G. Higgins, R. O. Hynes, *Mol. Biol. Cell* **2001**, *12*, 891.
- [15] Y. Kim, G. A. West, G. Ray, S. P. Kessler, A. C. Petrey, C. Fiocchi, C. McDonald, M. S. Longworth, L. E. Nagy, C. A. de la Motte, *Matrix Biol.* **2018**, *66*, 93.
- [16] B. Yang, Z. Liu, H. Liu, M. A. Nash, *Front. Mol. Biosci.* **2020**, *7*, 85.
- [17] A. Harder, A. K. Möller, F. Milz, P. Neuhaus, V. Walhorn, T. Dierks, D. Anselmetti, *Biophys. J.* **2015**, *108*, 1709.
- [18] S. N. Innes-Gold, J. P. Berezney, O. A. Saleh, *Biophys. J.* **2020**, *119*, 1351.
- [19] F. Bano, S. Banerji, M. Howarth, D. G. Jackson, R. P. Richter, *Sci. Rep.* **2016**, *6*, 34176.
- [20] F. Bano, M. I. Tammi, D. W. Kang, E. N. Harris, R. P. Richter, *Biophys. J.* **2018**, *114*, 2910.
- [21] D. J. Müller, J. Helenius, D. Alsteens, Y. F. Dufrêne, *Nat. Chem. Biol.* **2009**, *5*, 383.
- [22] L. A. Chtcheglova, P. Hinterdorfer, *Methods Mol. Biol.* **2013**, *950*, 359.
- [23] M. Delguste, G. L. Brun, F. Cotin, B. Machiels, L. Gillet, D. Alsteens, *Nano Lett.* **2021**, *21*, 847.
- [24] N. M. English, J. F. Lesley, R. Hyman, *Cancer Res.* **1998**, *58*, 3736.
- [25] J. Lesley, V. C. Hascall, M. Tammi, R. Hyman, *J. Biol. Chem.* **2000**, *275*, 26967.
- [26] J. Lesley, I. Gál, D. J. Mahoney, M. R. Cordell, M. S. Rugg, R. Hyman, A. J. Day, K. Mikecz, *J. Biol. Chem.* **2004**, *279*, 25745.
- [27] J. Schindelin, I. Arganda-Carreras, E. Frise, V. Kaynig, M. Longair, T. Pietzsch, S. Preibisch, C. Rueden, S. Saalfeld, B. Schmid, J.-Y. Tinevez, D. J. White, V. Hartenstein, K. Eliceiri, P. Tomancak, A. Cardona, *Nat. Methods* **2012**, *9*, 676.
- [28] H. J. Butt, M. Jaschke, *Nanotechnology* **1995**, *6*, 1.
- [29] C. Bustamante, J. F. Marko, E. D. Siggia, S. Smith, *Science* **1994**, *265*, 1599.
- [30] G. V. Dubacheva, C. Araya-Callis, A. Geert Volbeda, M. Fairhead, J. Codée, M. Howarth, R. P. Richter, *J. Am. Chem. Soc.* **2017**, *139*, 4157.
- [31] R. Peach, D. Hollenbaugh, I. Stamenkovic, A. Aruffo, *J. Cell. Biol.* **1993**, *122*, 257.
- [32] R. P. Richter, A. Brisson, *Langmuir* **2003**, *19*, 1632.
- [33] M. Sun, J. S. Graham, B. Hegedüs, F. Marga, Y. Zhang, G. Forgacs, M. Grandbois, *Biophys. J.* **2005**, *89*, 4320.
- [34] D. Raucher, M. P. Sheetz, *Biophys. J.* **1999**, *77*, 1992.
- [35] Z. Zheng, S. Katoh, Q. He, K. Oritani, K. Miyake, J. Lesley, R. Hyman, A. Hamik, R. M. Parkhouse, A. G. Farr, *J. Cell. Biol.* **1995**, *130*, 485.
- [36] G. I. Bell, *Science* **1978**, *200*, 618.
- [37] E. Evans, K. Ritchie, *Biophys. J.* **1997**, *72*, 1541.
- [38] P. Teriete, S. Banerji, M. Noble, C. D. Blundell, A. J. Wright, A. R. Pickford, E. Lowe, D. J. Mahoney, M. I. Tammi, J. D. Kahmann, I. D. Campbell, A. J. Day, D. G. Jackson, *Mol. Cell* **2004**, *13*, 483.
- [39] S. Banerji, A. J. Wright, M. Noble, D. J. Mahoney, I. D. Campbell, A. J. Day, D. G. Jackson, *Nat. Struct. Mol. Biol.* **2007**, *14*, 234.
- [40] P. M. Wolny, S. Banerji, C. Gounou, A. R. Brisson, A. J. Day, D. G. Jackson, R. P. Richter, *J. Biol. Chem.* **2010**, *285*, 30170.
- [41] S. A. Freeman, A. Vega, M. Riedl, R. F. Collins, P. P. Ostrowski, E. C. Woods, C. R. Bertozzi, M. I. Tammi, D. S. Lidke, P. Johnson, S. Mayor, K. Jaqaman, S. Grinstein, *Cell* **2018**, *172*, 305.
- [42] G. V. Dubacheva, T. Curk, R. Auzély-Velty, D. Frenkel, R. P. Richter, *Proc. Natl. Acad. Sci. U. S. A.* **2015**, *112*, 5579.
- [43] Z. T. Yew, M. Schlierf, M. Rief, E. Paci, *Phys. Rev. E.* **2010**, *81*, 031923.
- [44] H. Dietz, F. Berkemeier, M. Bertz, M. Rief, *Proc. Natl. Acad. Sci. U. S. A.* **2006**, *103*, 12724.
- [45] T. Suzuki, M. Suzuki, S. Ogino, R. Umamoto, N. Nishida, I. Shimada, *Proc. Natl. Acad. Sci. U. S. A.* **2015**, *112*, 6991.
- [46] D. G. Jackson, *Matrix Biol.* **2019**, *78–79*, 219.
- [47] D. G. Jackson, *Immunol. Rev.* **2009**, *230*, 216.
- [48] E. N. Harris, J. A. Weigel, P. H. Weigel, *J. Biol. Chem.* **2004**, *279*, 36201.
- [49] E. N. Harris, J. A. Weigel, P. H. Weigel, *J. Biol. Chem.* **2008**, *283*, 17341.

## SUPPORTING INFORMATION

Additional supporting information can be found online in the Supporting Information section at the end of this article.

**How to cite this article:** I. Garcia-Monge, A. Goodenough, C. C. Civaş, J. C. F. Kwok, R. P. Richter, *Proteoglycan Research* **2024**, *2*, e70002. <https://doi.org/10.1002/pgr2.70002>